Materials Science & Engineering C 96 (2019) 234–247

Contents lists available at ScienceDirect

Materials Science & Engineering C

journal homepage: www.elsevier.com/locate/msec

Superparamagnetic hybrid microspheres affecting osteoblasts behaviour

Tatiana M. Fernandes Patrício*, Silvia Panseri*, Monica Montesi, Michele Iafisco, Monica Sandri, Anna Tampieri, Simone Sprio

Institute of Science and Technology for Ceramics (ISTEC), National Research Council (CNR), Via Granarolo 64, 48018 Faenza, RA, Italy

ARTICLE INFO

Keywords:
Bio-inspired mineralisation
Hybrid microspheres
Iron-substituted apatite
Ions release
Cell behaviour
Bone tissue engineering

ABSTRACT

The present work describes biomimetic hybrid microspheres made of collagen type I-like peptide matrix (RCP) mineralised with Fe^{2+}/Fe^{3+} doping hydroxyapatite (RCPFeHA) by a bio-inspired process. Superparamagnetic RCPFeHA microspheres are obtained by emulsification of the hybrid slurries in the presence of citrate ions, to achieve a biomimetic surface functionalisation improving the bioactivity and the dispersion ability in cell culture medium. A biological in vitro study correlates the osteoblast cells behaviour to calcium and iron ions released by the hybrid microspheres in culture media mimicking physiological or inflammatory environment, evidencing a clear triggering of cell activity and bio-resorption ability. In presence of the microspheres, the osteoblast cells maintain their typical morphology and no cell damage were detected, whereas also showing up-regulation of osteogenic markers. The ability of the hybrid microspheres to undergo bio-resorption and release bioactive ions in response to different environmental stimuli without harmful effects opens new perspectives in bone regeneration, as magnetically active bone substitute with potential ability of drug carrier and smart response in the presence of inflammatory states.

1. Introduction

The regeneration of bone tissue claims the use of implantable devices with chemical composition and structure promoting the recruitment of autologous stem cells and differentiation towards osteogenic lineage with consequent new bone matrix deposition and substantial angiogenesis. Therefore, elective materials should promote physiological cell activity, whereas undergoing bio-degradation with adequate rate to not hamper new bone apposition and to limit any adverse effects related to the release of toxic degradation products [1–4].

Seeking for ideal biomaterials, previous studies have showed promising osteoinductive properties in collagen/hydroxyapatite hybrids, attested by the up-regulation of various bone-specific markers both in mesenchymal stem cells (MSCs) and in pre-osteoblast cells (MC3T3-E1) [5–8]. These hybrid constructs were obtained by bio-inspired mineralisation process where heterogeneous nucleation of mineral phases on self-assembling collagen occurs and is regulated by physico-chemical and ultrastructural control mechanisms, thus yielding high compositional and structural mimicry with natural bone tissue [9–11]. Such a process can be applied flexibly to tailor the mineralisation extent and to induce substitution of calcium with bioactive ions such as Mg^{2+}, Sr^{2+}, CO_3^{2-} in the hydroxyapatite structure to render the mineral phase closer to the bone composition, regulating the degradation profile and enhancing the bone cells activity [3,12–17].

Recent studies demonstrated that the selective doping with divalent and trivalent iron ions (Fe^{2+}/Fe^{3+}) confers intrinsic superparamagnetic properties to nanocrystalline hydroxyapatite (FeHA) and enhances its osteogenic character [18–20]. Bioactive magnetic materials elicit ever growing interest as therapeutic agents, due to their potential to guide the bone regeneration process by *on-demand* release of bioactive factors or by direct magnetic stimulation [17]. Enhanced osteogenic differentiation of mesenchymal stem cells, osteoblast adhesion and differentiation, as well as boosting bone tissue regeneration by magnetic fields were all described as main advantages of magnetic biomaterials that could give rise to a new generation of smart devices [17,21–26]. In this respect, considering the toxicity related to magnetic iron or gadolinium oxides, the use of biocompatible, bioactive magnetic phases such as FeHA is of great interest in the perspective to improve therapeutic effects in association to enhanced safety.

In a recent study, a bio-inspired mineralisation process was applied to obtain the heterogeneous nucleation of FeHA on collagen type I like peptide (RCP) matrix (RCPFeHA), resulting into superparamagnetic hybrids microspheres with bone-like composition and showing no cytotoxic effect on murine pre-osteoblasts cells (MC3T3-E1) [27]. Such microspheres were proposed as bone filler or as carrier of drugs or growth factors active in bone tissue regeneration. A typical drawback of magnetic materials is their aptitude to agglomerate into clusters, owing to strong magnetic dipole-dipole attractions and electrostatic repulsive

* Corresponding authors.
E-mail addresses: tatianamfp@gmail.com (T.M. Fernandes Patrício), silvia.panseri@istec.cnr.it (S. Panseri).

https://doi.org/10.1016/j.msec.2018.11.014
Received 18 January 2018; Received in revised form 10 September 2018; Accepted 9 November 2018
Available online 14 November 2018
0928-4931/

potential by the ions exposed on the surface [28,29], which may limit its potential use as injectable drug delivery systems [30]. Previous studies attempted to prevent aggregation of hydroxyapatite based materials, by surface modification with different molecules, such as L-lactic acid, poly(ε-caprolactone), ethylene glycol, polyethylenimine, glycosaminoglycans and poly(acrylic acid) [31–34]. In spite of their good biocompatibility, such polymers are not naturally present in the physiological environment and can elicit adverse effects by release of acidic functional groups when undergoing dissolution [35].

The present work describes the development of hybrid magnetic microspheres presenting innovative surface functionalisation with bioactive citrate ions, with the purpose to prevent physical agglomeration and enable extensive biologic characterisation by cell culture. Citrate is naturally present in bone where it accounts for about 5.5 wt% of the total organic component [36], playing a critical role in determining the structure and crystalline habitus of the inorganic phase of bone tissue and showing ability to complex the calcium ions and to control the size, shape and surface charge of synthetic hydroxyapatite nanocrystals. Citrate is a growth inhibitor of hydroxyapatite [37], hence, citrate functional groups are interesting candidate for surface functionalisation of apatite-based materials, to modulate crystal growth to bone-like levels and to modify the surface charge for enhanced control of rheological behaviour and dispersion ability [36,38–40].

In our work the effect of citrate on the dispersion and stability of hybrid microspheres in cell culture media is investigated by physicochemical, thermal and magnetic analyses, and optimized to obtain the best dispersion into cell culture medium. Degradation studies are carried out under physiological and inflammatory-mimicking pH conditions. MC3T3-E1 cell viability, damage, morphology, and the expression of osteogenic related markers are also investigated. The obtained results encourage the use of these new magnetic hybrid biomaterials as bioactive bone fillers or as micro-carriers for drug delivery system in bone tissue engineering.

2. Materials and methods

2.1. Raw materials

RCP, commercially available as Cellnest™ recombinant peptide based on human collagen type I, was provided by Fujifilm Manufacturing Europe B.V. (The Netherlands). The material is characterised by molecular weight of 51.7 kDa and isoelectric point of ≈10.02. All the reactants used in the present study, i.e. calcium hydroxide ($Ca(OH)_2$, ≥95%), phosphoric acid (H_3PO_4, 85%), iron(II) chloride tetrahydrate ($FeCl_2{\cdot}4H_2O$, ≥99%), iron(III) chloride hexahydrate ($FeCl_3{\cdot}6H_2O$, 97%), sodium hydroxide (NaOH, ≥98%), corn oil, acetone (≥99.9%), potassium bromide (KBr, ≥99%), phosphate buffered saline (PBS), HEPES sodium salt (≥99.5%), acetic acid (≥99.85%), sodium acetate (≥99%), were all purchased from Sigma Aldrich (St Louis, MO, USA), whereas nitric acid (HNO_3, 65%) was purchased from Titolchimica (Italy), and fluidMAG-CT (i.e. commercial magnetite nanoparticles, size 50 nm) from Chemicell (Germany, Berlin). Biological reactants were described in Section 2.6. Ultrapure water (0.22 mS, 25 °C) was used in all the experiments.

2.2. Synthesis of slurries

Iron-free and iron-containing mineralised slurries were obtained by a bio-inspired mineralisation process, based on heterogeneous nucleation of hydroxyapatite and Fe^{2+}/Fe^{3+} doped hydroxyapatite on RCP matrix, as previously described [27]. Briefly, for the preparation of the iron-containing mineralised slurries an aqueous solution of RCP (≈0.006 M) was prepared and mixed with an acidic H_3PO_4 solution (≈3.9 M), then poured dropwise into a basic aqueous suspension of $Ca(OH)_2$ (≈1.9 M) containing $FeCl_2{\cdot}4H_2O$ (≈1.56 M) and $FeCl_3{\cdot}6H_2O$ (≈1.04 M) as sources of Fe^{2+} and Fe^{3+} ions respectively, with an established molar ratio of 3:2, at $T = 60$ °C. The overall ion content was set to have a nominal Ca/P = 1.67 and Fe/Ca = 0.2. The process was carried out under magnetic stirring, to achieve a nominal mineralisation extent (i.e. inorganic:organic fraction) equal to 40 wt% and the final slurry contained 11 wt% of RCP. The as-obtained material was henceforth coded as RCPFeHA.

Iron-free mineralised slurries were synthesised similarly to RCPFeHA without adding any iron precursor in the $Ca(OH)_2$ suspension at two different temperatures of 20 °C and 60 °C, henceforth coded as $RCPHA_{RT}$ and RCPHA, respectively. $RCPHA_{RT}$ was synthesised for the microspheres production, and for the physical, chemical and biological characterisation; whereas RCPHA was prepared in the same conditions of RCPFeHA and is here used to evaluate the effect of iron substitution in the mineral phase.

The introduction of different concentrations of sodium citrate (i.e. 0.55 M, 0.3 M, 0.06 M, 0.006 M and 0.0006 M) in the RCPFeHA was investigated. Sodium citrate was added to the slurries and maintained under magnetic stirring for about 6 h, at room temperature (≈20 °C). The uptake of citrate ions onto the slurries was monitored by measuring the surface charge of the slurries at concentration of 0.55 M.

Slurry of RCP dispersed with commercial magnetite nanoparticles (fluidMAG-CT, Chemicell GmbH, 25 mg/mL) and a solution of pure RCP were also employed for the synthesis of microspheres (see next section) as control materials. RCP/magnetite slurry was prepared dropping 2 mL of fluidMAG-CT suspension in a RCP solution (5 g in 12 mL of Milli-Q water), under magnetic stirring for 30 min, at 40 °C. The as-obtained material was encoded as RCPfluidMAG-CT. The pure RCP solution was prepared dissolving 5 g of RCP in 12 mL of Milli-Q water under magnetic stirring at about 40 °C.

2.3. Fabrication of microspheres by emulsification process

A water-in-oil emulsification process was used to produce microspheres based on pure RCP, RCPfluidMAG-CT and mineralised slurries (i.e. $RCPHA_{RT}$, RCPHA and RCPFeHA), as previously described [27] (Table 1). Briefly, 20 g of slurry or solution was dropped in 45 g of prewarmed corn oil and kept under mechanical stirring for 20 min. The as-obtained mixture was cooled, until microspheres gelling, and dropped into a 300 mL of chilled acetone and kept under mechanical stirring for 5 min, then maintained for 1 h at room temperature, under mechanical stirring. The microspheres were left to sediment and acetone was carefully removed; then 300 mL of clean acetone was added and the microspheres were washed for 10 min. This step was repeated twice. The microspheres were filtered, dried overnight in an oven at 40 °C, and

Table 1
Composition of the as-synthesised microspheres.

Composition of microspheres	Code
Collagen type I based recombinant peptide	RCP
Collagen type I based recombinant peptide synthesised with commercial superparamagnetic nanoparticles	RCPfluidMAG-CT
Collagen type I based Recombinant Peptide mineralised with hydroxyapatite nanophase (synthesis at 20 °C)	$RCPHA_{RT}$
Collagen type I based Recombinant Peptide mineralised with hydroxyapatite nanophase (synthesis at 60 °C)	RCPHA
Collagen type I based Recombinant Peptide mineralised with iron doped hydroxyapatite (synthesis at 60 °C)	RCPFeHA

sieved to achieve a size distribution within the range of 50 to 75 μm. Three different batches of each type of microspheres were produced. Then, microspheres were crosslinked by using dehydrothermal treatment (DHT) at 160 °C for 48 h under vacuum.

2.4. Morphological, physicochemical and magnetic characterisation

The surface charge of functionalised slurries and microspheres was evaluated in terms of ζ-potential (Zetasizer Nano analyser; Malvern, UK). ζ-potential measurements through electrophoretic mobility were carried out by using disposable folded capillary cells (DTS1061; Malvern, UK) at 25 °C. For functionalised slurries, 100 μL of slurry was diluted in 5 mL of Milli-Q water and ζ-potential was evaluated at $t = 0$ and $t = 30$ min, 90 min, 3 h and 6 h. Microspheres surface charge was evaluated in HEPES buffer (i.e. 0.01 M; pH 7.4) at concentration of 1.2 mg/mL. The ζ-potential average was calculated from three separate measurements (100 runs each) for each type of microspheres and the results were shown as Mean ± Standard Error (SEM).

The morphology of the microspheres was investigated by using Scanning Electron Microscope (SEM) (FEI Quanta 600, USA) in low vacuum mode with an accelerating voltage of 10 kV and a working distance of 10 mm. Size distribution of microspheres was evaluated by SEM micrographs and analysed by Image J software.

The identification of functional groups in the mineralised materials was assessed by Fourier Transform Infrared Spectroscopy (FTIR) (Avatar 320 FT-IR, Thermo Nicolet, Canada). The infrared spectra were collected in the wavelength range from 400 to 4000 cm^{-1} with 2 cm^{-1} of resolution, using the KBr pellet technique. The sample (≈2 mg) was mixed with ≈150 mg of anhydrous KBr and the powder was pressed at 8000 psi into 7 mm diameter pellets.

The phase composition of the all as-produced microspheres was obtained by X-ray powder diffraction (XRD, D8 Advance, Bruker, Karlsruhe, Germany) acquired by using Cu-Kα radiation (λ = 1.54178 Å) generated at 40 kV and 40 mA, using a step-scanning method with a step size of 0.02° and a counting time of 0.5 s.

The overall content of calcium (Ca), phosphorus (P) and iron (Fe) was determined by inductively coupled plasma optical emission spectrometry (ICP-OES; Liberty200, Varian, Clayton South, Australia). Each type of material was prepared in triplicate by dissolving 20 mg of powder in 2 mL of HNO_3 (65 wt%) and the volume of the solution was raised to 100 mL by adding deionized water. Predetermined concentrations of Ca, P and Fe elements were prepared and used as standard calibration.

Simultaneous thermogravimetric (TGA) analysis (STA 449/C Jupiter, Netzsch, Germany) was carried out to assess the effect of citrate ions on thermal decomposition profile of RCPFeHA microspheres. 10 mg of microspheres were placed into an alumina crucible and the experiment was conducted in air flux with heating ramp from 30 °C to 1100 °C and heating rate of 10 °C/min.

Vibrating sample magnetometer (VSM) Lakeshore 735, in the range from −15 KOe to 15 KOe was used to evaluate the magnetic properties of RCPFeHA. A predetermined amount of RCPFeHA was loaded into the sample holder and the experiments were carried out at room temperature. The results are presented with uncertainty of about ± 2%.

2.5. Microspheres degradation study

Microspheres degradation tests were carried out in two different conditions that mimic i) physiological (pH 7.4) and ii) inflammatory (pH 5.0) environment. For physiological condition, osteogenic differentiation medium was prepared with DMEM (Gibco), 10% Fetal Bovine Serum (FBS), 1% penicillin-streptomycin (100 U/mL-100 μg/mL), 10 mM β-glycerophosphate and 50 μg/mL ascorbic acid. The inflammatory-like condition was achieved by buffering the previous medium with sterile sodium acetate-acetic acid buffer solution, reaching pH 5.0. These as-prepared media were encoded as DMEM and DMEM-IM, respectively.

Each type of microspheres was sterilised in PBS 1X by using autoclave (120 °C for 20 min). Then PBS 1X was substituted by DMEM or DMEM-IM obtaining a final concentration of 30 mg/mL of microspheres. Three samples of each type of microspheres were investigated. DMEM or DMEM-IM only, were used as controls. Microspheres degradation study was carried out under incubation at 37 °C in an atmosphere of 5% CO_2, over a period of 28 days.

Microspheres morphology were evaluated by SEM, after 7, 14, 21 and 28 days. Moreover, $RCPHA_{RT}$ and RCPFeHA at day 28 were washed four times with Milli-Q water, freeze dried and stored for further FTIR and XRD characterisations.

2.5.1. Evaluation of ions adsorption and dissolution

The amount of Ca and Fe ions released from RCPfluidMAG-CT, $RCPHA_{RT}$ and RCPFeHA in DMEM and DMEM-IM was evaluated by ICP-OES. At scheduled time points (i.e. 12 h, 24 h, 48 h, 7 days, 14 days, 21 days and 28 days), both media were separated from microspheres by centrifugation (13,300 rpm, for 12 min), and tested to quantify the released ions and to measure the pH values (XS instruments, Italy). DMEM and DMEM-IM were replaced at the as-mentioned time points. The retrieved media (0.6 mL) were digested into 1 mL of HNO_3 (65 wt %) and the volume of the solution was raised to 3 mL by adding deionized water, and further analysed by ICP-OES. DMEM was a medium enriched of calcium ions (≈1.05 mM) and the percentage of adsorbed calcium at each time point was normalized to the total calcium in the replaced media, while released ions were normalized to the total concentration of each element (i.e. Ca_{total} and Fe_{total}) in 30 mg of microspheres. Three samples per type of microspheres were used and the ions concentration was expressed as Mean ± SEM.

2.6. Biological characterisation

2.6.1. Cell culture

Mouse pre-osteoblast cell line, MC3T3-E1 Subclone 14 (ATCC cell bank, Manassas, VA, USA) was used for the biological investigation. In detail, MC3T3-E1 cells were cultured in αMEM without ascorbic acid (Gibco), 10% FBS and 1% penicillin-streptomycin (100 U/mL–100 μg/mL). Cell culture was kept at 37 °C in an atmosphere of 5% CO_2, later the cells were detached from culture flasks by trypsinization, centrifuged and re-suspended in cell medium. Cell number and cell viability were assessed by trypan-blue dye exclusion test.

For the experiment, cells were plated in cell culture plates at a density of 2500 cells/cm^2 in osteogenic medium (αMEM, 10% FBS, 1% penicillin-streptomycin (100 U/mL–100 μg/mL), 10 mM β-glycerophosphate, 50 μg/mL ascorbic acid) 24 h after cells seeding, different concentrations of each sterilised microspheres (i.e. 10 μg/mL, 100 μg/mL and 500 μg/mL of RCP, RCPfluidMAG-CT, $RCPHA_{RT}$ and RCPFeHA) were added to the cell culture. All the cell-handling procedures were performed in a sterile laminar flow hood and all cell-culture incubation steps were performed at 37 °C with 5% CO_2.

2.6.2. Cell viability analysis

Cell viability as function of cell number based on metabolic activity was evaluated by XTT assay, following the manufacture's protocol (Thermo Fisher Scientific, U.S.A.). Briefly, 6 mg of XTT was dissolved in 6 mL of osteogenic cell medium and then was added 15 μL of 10 mM of phenazine methosulfate (PMS) solution. After, 75 μL of the as-prepared solution was dropped in each well and incubated at 37 °C in CO_2 incubator for 2 h and the absorbance was analysed at 450 nm by using a Multiskan FC Microplate Photometer (Thermo Fisher Scientific, USA). Cell viability was analysed after 1, 3 and 7 days of cell seeding. The experiments were conducted in triplicates and plotted as Mean ± SEM.

2.6.3. Cell morphology and cell damage evaluation

2.6.3.1. Actin filament staining. At day 3, cell morphology was evaluated by phalloidin staining. Cells were washed with PBS 1X for 5 min, fixed with

4% (w/v) paraformaldehyde for 15 min. Permeabilization was performed with PBS 1X with 0.1% (v/v) Triton X-100 for 5 min. Then, 38 nM of FITC-conjugated phalloidin (Invitrogen, U.S.A.) in PBS 1X was added and was remained at room temperature in the dark for 20 min. For nuclear staining the cells were incubated with 300 nM of DAPI for 5 min. Cells only were used as internal control. Images were acquired by an Inverted Ti-E fluorescence microscope and one sample per group was analysed.

2.6.3.2. Hematoxylin and eosin staining (H&E). After 3 days of cell culture, cells were washed with PBS 1X for 5 min, fixed with 4% (w/v) of formaldehyde for 15 min, then washed twice with PBS 1X for 5 min and stained with H&E. Briefly, the cells were stained with Mayer's hematoxylin for 7 min and then were differentiated with tap water for 10 min. After, the cells were stained with eosin Y (0.25%) for 30 s, washed with Milli-Q water and mounted. Cells only were used as internal control. Images were acquired by an Inverted Ti-E fluorescence microscope and one sample per group was analysed.

2.6.3.3. Apoptotic cells. After 24 h and 72 h of incubation, cells were evaluated with Annexin V/Dead Cell Apoptosis Kit (Molecular Probes) according to manufacturer's instructions. Briefly, cells were washed with cold PBS 1X, and incubated with 1X annexin-binding buffer, Alexa Fluor 488 annexin V and propidium iodide (PI) working solution for 15 min at room temperature following by DAPI staining for cell nuclei. Cells incubated with Doxorubicin (1 μM DOX) were used as positive control. One sample per group was analysed and images were acquired with an inverted Ti-E fluorescence microscope (Nikon).

2.6.3.4. Reactive oxygen species (ROS). ROS formation at 24 h and 72 h was analysed by ROS indicator kit (carboxy-2,7-difluorodihydrofluorescein diacetate, carboxy-H2DFFDA, Molecular Probes), according to manufacturer's instructions. Briefly, cells were incubated with ROS detection reagent for 15 min at 37 °C, then this solution was removed and cell culture medium was added for 10 min at 37 °C, before washing the cells with PBS 1X following by DAPI staining for cell nuclei. Cells incubated with 100 μM of hydrogen peroxide (H_2O_2) were used as positive control. One sample per group was analysed and images were acquired with an inverted Ti-E fluorescence microscope.

2.6.4. Western blot analysis

After 7 days of culture the cells with 100 μg/mL of microspheres, the cells were lysed in a Radioimmunoprecipitation buffer (RIPA buffer) supplemented with a proteinase inhibitor cocktail (Cell Signalling Technology, U.S.A.). The protein concentration in each cell lysate supernatant was determined by a colorimetric assay (Kit DC Protein Assay, Bio-Rad, U.S.A.). The protein samples were loaded and separated in a 4–20% Mini-PROTEAN TGX stain-free protein gels (Bio-Rad, U.S.A.), using a Mini-PROTEAN electrophoresis cell kit (Bio-Rad, U.S.A.). Proteins were then transferred to a nitrocellulose membranes by means of a Trans-Blot Turbo™ transfer system (Bio-Rad, U.S.A.), with the blots incubated thereafter for 30 min at room temperature in a blocking solution of 2.5% non-fat dry milk in PBS 1X. The membranes were incubated overnight at 4 °C with primary rabbit antibody anti-alkaline phosphatase (ALP, Abcam, UK), anti-osteocalcin (LifeSpan BioSciences, U.S.A.) and anti-β-actin (Cell Signaling Technology, USA) as internal control. Moreover, rabbit antibody anti-LC3B-I and LC3B-II (Cell Signalling Technology, USA) was used to detect autophagy, as cellular stress marker. Then membranes were incubated with a horseradish goat peroxidase-linked secondary antibody anti-rabbit (Bio-Rad, U.S.A.) for 1 h 30 min. An enhanced chemiluminescence kit (ECL, Bio-Rad, U.S.A.) was used to visualize the protein bands with ChemiDoc XRS + (Bio-Rad, U.S.A.). In order to evaluate the relative protein expression, the ALP, osteocalcin and LC3B-I and LC3B-II band intensities were quantified by densitometry using ImageLab Software and were then normalized over the signal of the corresponding bands of β-actin.

2.6.5. Quantitative real-time polymerase chain reaction (qPCR)

The relative quantification of the gene expression profile of MC3T3-E1 cells, cultured for 7 days with 100 μg/mL of microspheres, was assessed by qPCR. Total RNA was harvested by using Tri Reagent, followed by the Direct-zol RNA MiniPrep kit (Zymo Research) according to manufacturer's instructions. RNA integrity was analysed by native agarose gel electrophoresis and the quantification was performed by using the Qubit® 2.0 Fluorimeter together with the Qubit® RNA BR assay kit, according to the manufacturer's instructions (Invitrogen, U.S.A.). Total RNA (500 ng) was reverse transcribed to cDNA using the High-Capacity cDNA Reverse Transcription Kit, according to manufacturer's instructions (Applied Biosystems, U.S.A.). The relative quantification of the expression of the genes, i.e. osteonectin (SPARC, Mn00486332-m1), osteocalcin (BGLAP, Mm00649782_gH), collagen I (COL I, Mm00483888_m1) and glyceraldehydes-3-phosphate dehydrogenase (GAPDH, Mm99999915_g1), used as housekeeping gene, were performed by StepOne™ Real-Time PCR System (Applied Biosystems, U.S.A.). Data were collected using the OneStep Software (v.2.2.2) and relative quantification was performed using the comparative threshold (CT) method (ΔΔCT) where the relative gene expression level equals $2^{-\Delta\Delta Ct}$ [41]. Experiments were performed in duplicate, using three technical replicates for each experiment and the results were normalized to RCP used as calibrator. Error bars reflect one standard deviation of the mean of three technical replicates, as described elsewhere [42,43].

2.7. Statistical analysis

Statistical analyses were performed by using GraphPad Prism 5 software. The unpaired *t*-test was used for ions release and two-way ANOVA, followed by Bonferroni post-tests was used for calcium adsorption in DMEM. Data is plotted as Mean ± SEM of n. 3 samples per each group.

Statistical analysis of biological tests was performed by using two-way ANOVA followed by Bonferroni post-tests for XTT analysis and data was plotted as Mean ± SEM of n. 3 samples per each group. All the other biological results were evaluated by one-way ANOVA followed by Tukey's multiple comparison test and data were plotted as Mean ± SEM of n. 2 samples per each group. Results were considered statistically significant when $p < 0.05$.

3. Results

3.1. Effect of citrate ions in the production of RCPFeHA microspheres

RCPFeHA slurry was enriched with citrate ions in order to modify its surface charge, to increase mutual repulsive interactions and prevent agglomeration. In a first step, the effect of sodium citrate (with concentration of 0.55 M) as a function of time was evaluated by measuring the ζ-potential at scheduled time points. By increasing the time of magnetic stirring, the negative surface charge of the slurry was enhanced by the adsorption of citrate ions onto the mineral phase and the highest negative surface charge (about −18 mV) was obtained at 90 min (Table SI1). In a second step, RCPFeHA slurry was functionalised with sodium citrate at various concentrations for 90 min, then microspheres were produced by emulsification process (Fig. 1A). RCPFeHA microspheres generated without the addition of citrate in the slurry appeared highly agglomerated after contact with osteogenic differentiation medium (Fig. 1B). Also, the employment of high quantity of sodium citrate (i.e. 0.55 M) induced microspheres agglomeration (up to 1 mm in size), while by decreasing the citrate concentration, smaller aggregates of microspheres were generated (Fig. 1C–G). In particular, microspheres prepared with the slurry functionalised with 0.006 M of sodium citrate were well dispersed (i.e. no aggregation occurred) (Fig. 1F) and resulted stable for at least 7 days in osteogenic differentiation medium (Fig. 1H).

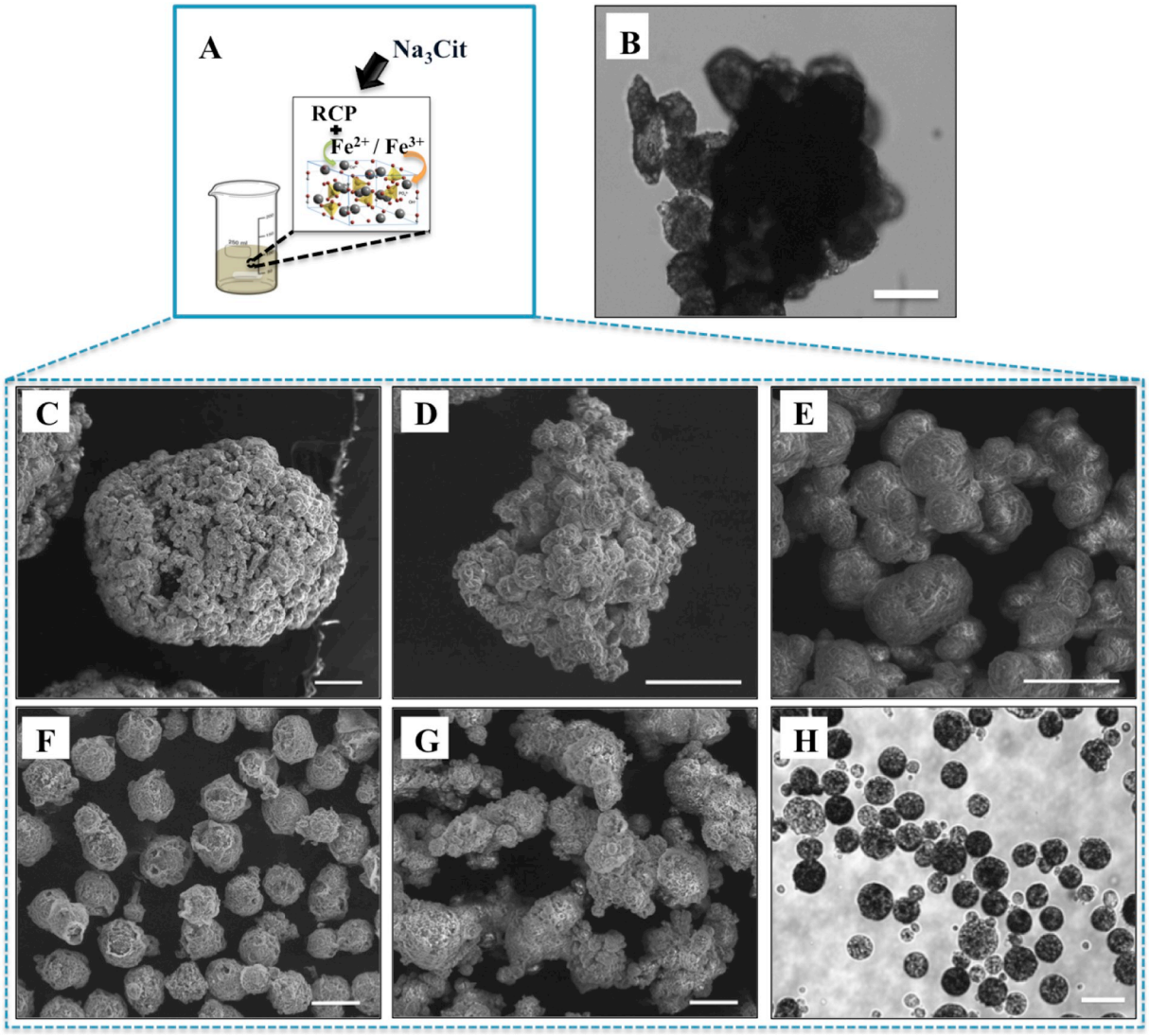

Fig. 1. Effect of sodium citrate concentration on the RCPFeHA microspheres. A) Designed set-up of functionalisation of RCPFeHA slurry with sodium citrate; B) Optical micrograph of microspheres generated without the addition of citrate in the slurry dispersed in osteogenic differentiation medium, (Scale bar: 100 μm); SEM images of microspheres obtained by using RCPFeHA slurry functionalised with various concentrations of sodium citrate: C) 0.55 M (Scale bar: 200 μm); D) 0.28 M; E) 0.06 M; F) 0.006 M; G) 0.0006 M. H) Optical micrograph of microspheres generated with RCPFeHA slurry functionalised with 0.006 M in presence of osteogenic differentiation medium, (Scale bar: 100 μm).

The effect of addition of 0.006 M sodium citrate in the slurry on the chemical and thermal features of RCPFeHA microspheres was evaluated by FT-IR and TGA analysis (Fig. 2), respectively. The FT-IR spectra of RCPFeHA microspheres prepared in presence and in absence of citrate report the typical vibration peaks of RCP (i.e. amide I, amide II, amide III and carboxylic groups) and confirm the formation of poorly crystalline and B-type carbonated hydroxyapatite (Fig. 2A). In the case of citrate-functionalised microspheres, FT-IR analysis clearly shows the absorption band at 1755 cm^{-1} attributed to the stretching C═O vibrations from −COOH group of sodium citrate (Fig. 2A, marked with asterisk), thus confirming the effective adsorption of citrate ions, whereas other vibration modes of citrate (i.e. at 1600, 1450 and 1387 cm^{-1}, as also previously indicated by other works [44,45]) are overlapped by the RCP signals.

In Fig. 2B the thermogravimetric curves of non-functionalised and citrate-functionalised RCPFeHA microspheres before and after cross-linking are reported. The weight loss below to ≈140 °C is assigned to the evaporation of physically adsorbed water molecules, then the degradation of RCP matrix occurs up to ≈600 °C, and finally the evaporation of carbonate and hydroxyl ions contained in the apatite phase proceeds up to 1000 °C. By comparing non-functionalised with functionalised RCPFeHA, slight differences related to the weight loss (≈7 wt%) in the range ≈400 °C–600 °C, are assigned to the decomposition of citrate ions. Overall, these data revealed that the DHT treatment did not influence the interaction of RCP with the mineral phase, nor the linking of citrate ions to the mineral phase, as showed by the FT-IR and the TGA spectra.

3.2. Characterisation of optimized microspheres

Hybrid slurries (i.e. $RCPHA_{RT}$, RCPHA and RCPFeHA) were functionalised with 0.006 M of sodium citrate, and then were engineered into microspheres by emulsification process. Subsequently, the phase composition of the as-produced microspheres (i.e. RCP, RCPfluidMAG-CT, $RCPHA_{RT}$, RCPHA, RCPFeHA) was analysed by XRD (Fig. 3).

In RCP and RCPfluidMAG-CT, a broad diffraction profile in the 10–30 2Θ° range is attributed to the organic phase characterised by amorphous structure. In RCPHA and RCPFeHA, both synthesised at 60 °C, hydroxyapatite phase was detected (in agreement with the JCPDS card number: 09–0432), presenting low crystallinity degree, as

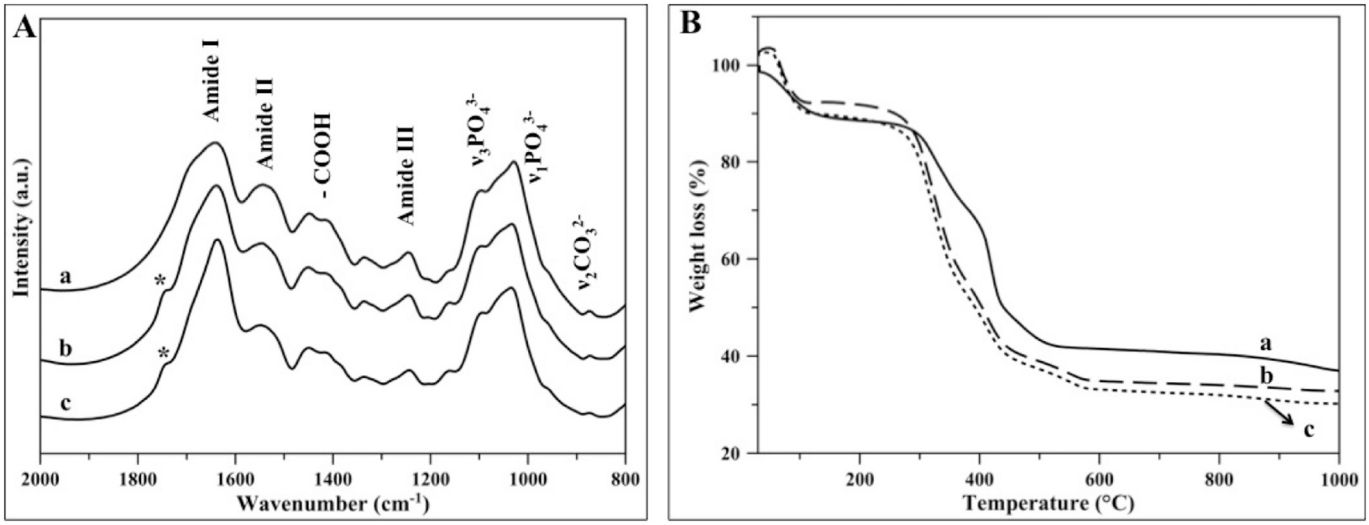

Fig. 2. Chemical and thermal features of functionalised RCPFeHA microspheres, evaluated by (A) FT-IR and (B) TGA analysis: (a) Non-functionalised RCPFeHA microspheres; (b) Functionalised RCPFeHA microspheres and (c) crosslinked by DHT.

suggested by the broadening of the XRD peaks. The synthesis of $RCPHA_{RT}$ at 20 °C yielded hydroxyapatite phase featuring even lower crystallinity degree, as evidenced by the broader diffraction peaks, ascribed to the lower synthesis temperature limiting the crystal organization. The low crystallinity degree of the mineralised matrices was corroborated by the low value of their splitting factor (SF) [46,47] obtained by FTIR spectra, i.e. $RCPHA_{RT}$ = 2.34, RCPHA = 2.39 and RCPFeHA = 2.25. The slight shift of the diffraction peaks (Fig. 3e, black arrow) and the reduction of the crystallinity in RCPFeHA (Fig. 3e) compared to RCPHA suggested the effective partial replacement of Ca ions for Fe ions into the hydroxyapatite lattice, inducing lattice distortion [18].

Two different magnetic materials were produced, RCPfluidMAG-CT and RCPFeHA. In the XRD pattern of RCPfluidMAG-CT, the presence of the peak at 35.4° (corresponding to the (311) plane of iron oxide, JCPDS card number: 01-079-0417), confirmed the presence of magnetite. In the case of RCPFeHA the presence of Fe^{2+}/Fe^{3+} ions and the synthesis temperature > 40 °C induced the heterogeneous nucleation of a low amount of iron oxide phase as revealed by the presence of the diffraction peak at 2θ° ≈ 35.4 corresponding to the (311) plane of iron oxide (JCPDS card number: 01-079-041) (Fig. 3A). In a previous study this phase was identified as maghemite nucleated onto the apatite structure by Extended X-Ray Absorption Fine Structure (EXAFS analysis) and Mössbauer Spectroscopy [19]. RCPFeHA presents superparamagnetic like-behaviour as described in the Fig. 3B, with specific magnetisation of 1.65 emu/g.

SEM analysis shows that microspheres present spherical shape, with the exception of RCPHA (Fig. 4). The adopted synthesis temperature (i.e. 60 °C) during the biomineralisation process of RCPHA, promoted the formation of slurry with low viscosity, so that in the subsequent emulsification process it was not adequately viscous for well-defined microspheres production. As also suggested by previous studies [48], the low viscosity can be related to the relatively high crystallinity of hydroxyapatite, ascribed to the higher synthesis temperature (i.e. 60 °C), in respect to the other samples investigated in this work, (see also Fig. 3).

RCP and RCPfluidMAG-CT microspheres feature smooth surface, while the rougher surface of $RCPHA_{RT}$ and RCPFeHA microspheres was related to the homogeneous distribution of the mineral phase. The size distribution of RCP, RCPfluidMAG-CT, $RCPHA_{RT}$ and RCPFeHA

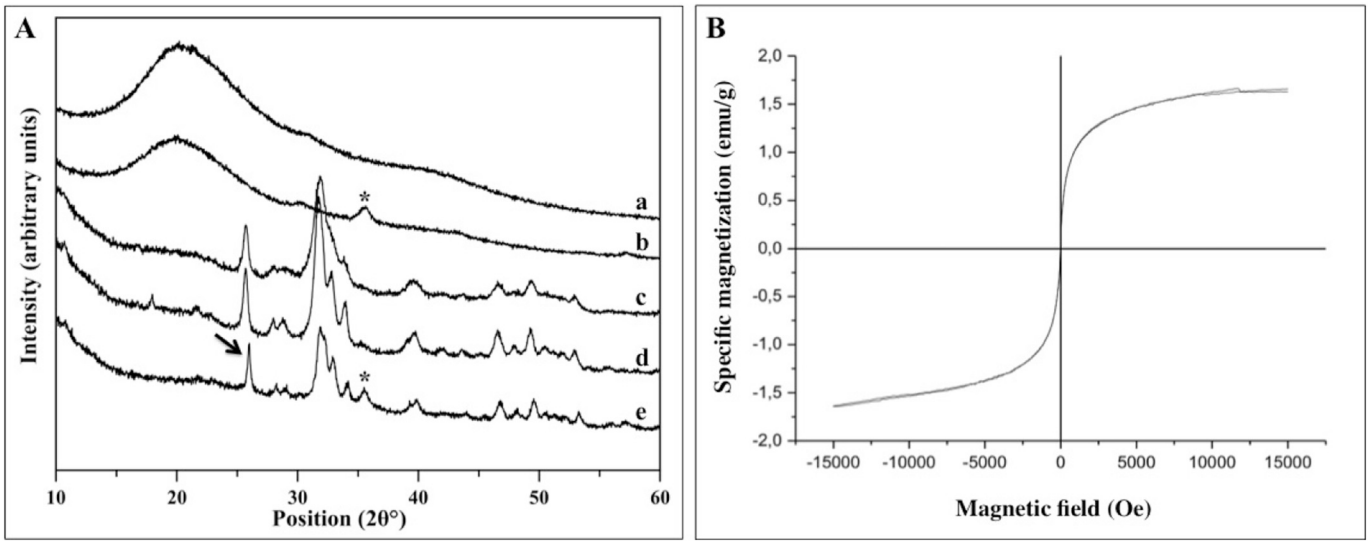

Fig. 3. A) XRD pattern of the as-obtained microspheres: RCP (a); RCPfluidMAG-CT (b); $RCPHA_{RT}$ (c); RCPHA (d); RCPFeHA (e). (Iron oxide formation is indicated by *). B) Magnetic properties of RCPFeHA obtained by VSM.

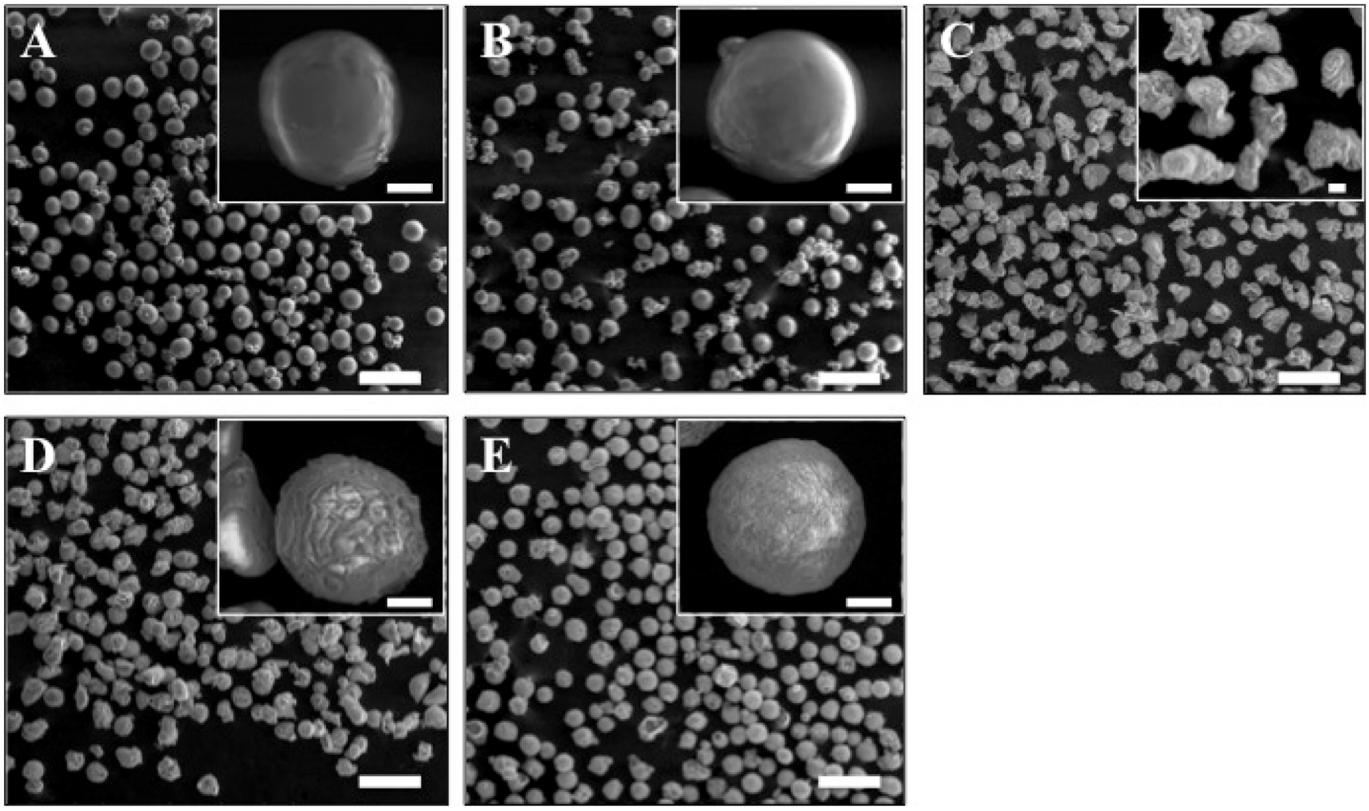

Fig. 4. SEM micrographs from the as-produced microspheres: A) RCP; B) RCPfluidMAG-CT; C) RCPHA; D) $RCPHA_{RT}$; E) RCPFeHA, (Scale bar is 200 μm and in the figure inserts is 20 μm).

microspheres was evaluated by SEM micrographs and analysed by Image J software. Size distribution and related microspheres size obtained by Gaussian distribution (Fig. SI1) reveal similar size for all samples, i.e. ≈70 μm.

The elemental composition of microspheres is presented in Table 2. The differences in (Fe + Ca)/(P + CO_3^{2-}) molar ratio for RCPFeHA, compared to Ca/P molar ratio of stoichiometric hydroxyapatite (≈1.67), can be related to the incorporation of foreign ions into the apatite structure, as well as possible free ions linked to RCP structure [27].

As previously was mentioned $RCPHA_{RT}$ and RCPFeHA were functionalised with 0.006 M of sodium citrate. Citrate ions complex the calcium ions in $RCPHA_{RT}$ and negative surface charge was obtained (−3.34 ± 0.05 mV). Moreover, the functionalisation with sodium citrate in RCPFeHA provokes the increase of the surface charge from 2.17 ± 0.63 mV (no citrate) to 5.86 ± 0.11 mV (with citrate), thus resulting much more stable in suspension or in contact with cell culture medium (Table 2).

3.3. Microspheres degradation studies under physiological and inflammatory-mimicking conditions

Various aspects are relevant to investigate during the degradation of the microspheres, such as surface morphology, pH, adsorption and release of ions in the media. RCP, RCPfluidMAG-CT, $RCPHA_{RT}$ and RCPFeHA microspheres were separately immersed in two different media: DMEM (pH 7.4) and DMEM-IM (pH 5) at 37 °C, during 28 days. The surface morphology was assessed by SEM micrographs after 7, 14, 21 and 28 days (Figs. 5 and 6).

All the tested microspheres show good stability in both media. Moreover, the beginning of the degradation of the microspheres was observed at day 28 (Figs. 5 and 6). In fact, at pH 7.4, microspheres present wrinkled structure and RCPFeHA shows a rough surface (Fig. $5D_{28D}$, figure insert), while at pH 5, the on-going dissolution of the mineral phase in $RCPHA_{RT}$ (Fig. 6C) and in RCPFeHA is clearly evident by the wrinkled structure (Fig. 6D).

The pH of the solutions, the adsorption and release of ions were investigated at predetermined time points (i.e. at 12 h, 24 h, 48 h and at day 7, 14, 21 and 28).

No significant differences were detected by comparing the measured pH in the controls (i.e. free-microspheres media) or in the media containing RCP or RCPfluidMAG-CT, at both pH conditions (Fig. SI2). On the other hand, higher pH values from DMEM in presence of $RCPHA_{RT}$ (Fig. SI2) were ascribed to higher calcium adsorption (about 80% at each time point) in the first 7 days, followed by a decrease to ≈16% at day 21. From day 21 to 28, a slight increase of calcium adsorption was

Table 2
ζ-potential and chemical elements of the microspheres, (*obtained by ICP-OES and §TGA analysis).

Code	ζ-potential, mV	* Ca, mol	* Fe, mol	*§Ca/(P + CO_3^{2-}), mol	*§(Fe + Ca)/(P + CO_3^{2-}), mol
RCP	1.53 ± 0.21	–	–	–	–
RCPfluidMAG-CT	2.20 ± 0.78	–	0.02 ± 0.01	–	–
$RCPHA_{RT}$	−3.34 ± 0.05	0.51 ± 0.01	–	2.03 ± 0.03	–
RCPFeHA	5.86 ± 0.11	0.48 ± 0.04	0.09 ± 0.01	–	2.31 ± 0.02

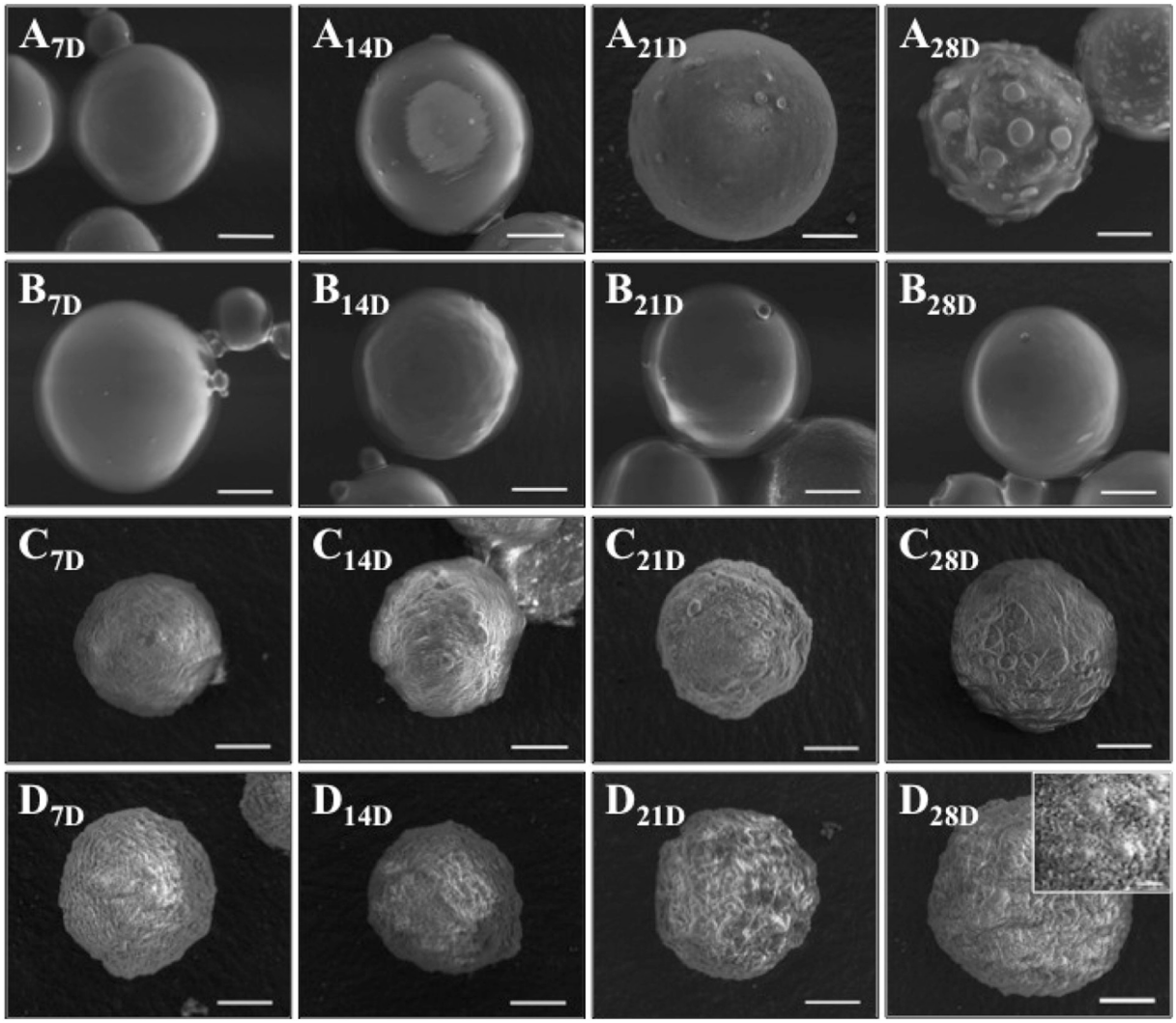

Fig. 5. SEM micrographs of microspheres, after immersion in DMEM at pH = 7.4, over 28 days. A) RCP; B) RCPfluidMAG-CT; C) $RCPHA_{RT}$; D) RCPFeHA, (Scale bar: 20 μm and 10 μm in the figure insert); (Note: 7D: 7 days; 14D: 14 days; 21D: 21 days; 28D: 28 days).

again detected (Fig. 7A), possibly due to the microspheres dissolution, as previously shown in Fig. 5.

In RCPFeHA about ≈50 to 90% of calcium was adsorbed during the test, reaching the saturation after 7 days in the presence of DMEM (Fig. 7A). Meanwhile, about 0.13 mM of Fe ions was released from RCPFeHA microspheres (Fig. 7B). At both conditions with RCPFeHA, significant differences on Fe ions release were shown ($p < 0.05$), indicating the exchange of iron ions to the adsorbed calcium ions in DMEM (Fig. 7B).

During 28 days at ≈pH 5, a slight increase in the pH of the medium in contact with $RCPHA_{RT}$ and RCPFeHA was observed, probably due to degradation of the microspheres and the release of ions (Fig. SI2; Fig. 7C). Moreover, the cumulative calcium release from $RCPHA_{RT}$ and RCPFeHA do not significantly differ (Fig. 7C). For RCPfluidMAG-CT in both media, extremely statistically significant differences on Fe release are showed ($p \leq 0.001$), indicating that in acidic pH, the release of Fe occurs faster (Fig. 7D).

The phase composition of $RCPHA_{RT}$ and RCPFeHA microspheres, after 28 days in both conditions (i.e. physiological and inflammatory), were also analysed by FTIR and XRD tests (Fig. 8). In agreement with SEM micrographs, FTIR and XRD spectra confirm the presence of organic matrix and the inorganic apatite phase in $RCPHA_{RT}$ and RCPFeHA, as reported by the vibration assignments in amide and phosphate groups, respectively (Fig. 8A). Moreover, XRD patterns show that no secondary phases formed after 28 days in neutral or acidic conditions, however clues indicating the degradation of the inorganic phase come from the XRD spectrum of RCPFeHA, showing broader and lower intensity diffraction peaks (Fig. 8B, C).

3.4. Biological characterisation

3.4.1. Cell viability

Microspheres were added to the cell cultures at 3 different concentrations (10 μg/mL, 100 μg/mL, 500 μg/mL). After 7 days, qualitative bright-field images showed a layer of cells well attached to the well-plate surfaces indicating the absence of high level of cytotoxicity (Fig. 9A). This data was also confirmed by XTT test. In fact, cell viability showed an increase of metabolic active cells over the experimental time even at the higher concentration of microspheres (Fig. 9B). In detail the 10 μg/mL microspheres concentration displayed no differences among the groups except for the day 7, when the cell viability was reduced in RCPfluidMAG-CT, $RCPHA_{RT}$ and RCPFeHA groups compared to RCP group. With 100 μg/mL of microspheres concentration, statistically significant differences were detected only at day 3. Also, here the RCPfluidMAG-CT and $RCPHA_{RT}$ groups were reduced compared to RCP group (Fig. 9B). So, probably this result was ascribable to the ion release from RCPfluidMAG-CT, $RCPHA_{RT}$ and RCPFeHA. The cell viability with the higher microspheres concentration had different behaviour

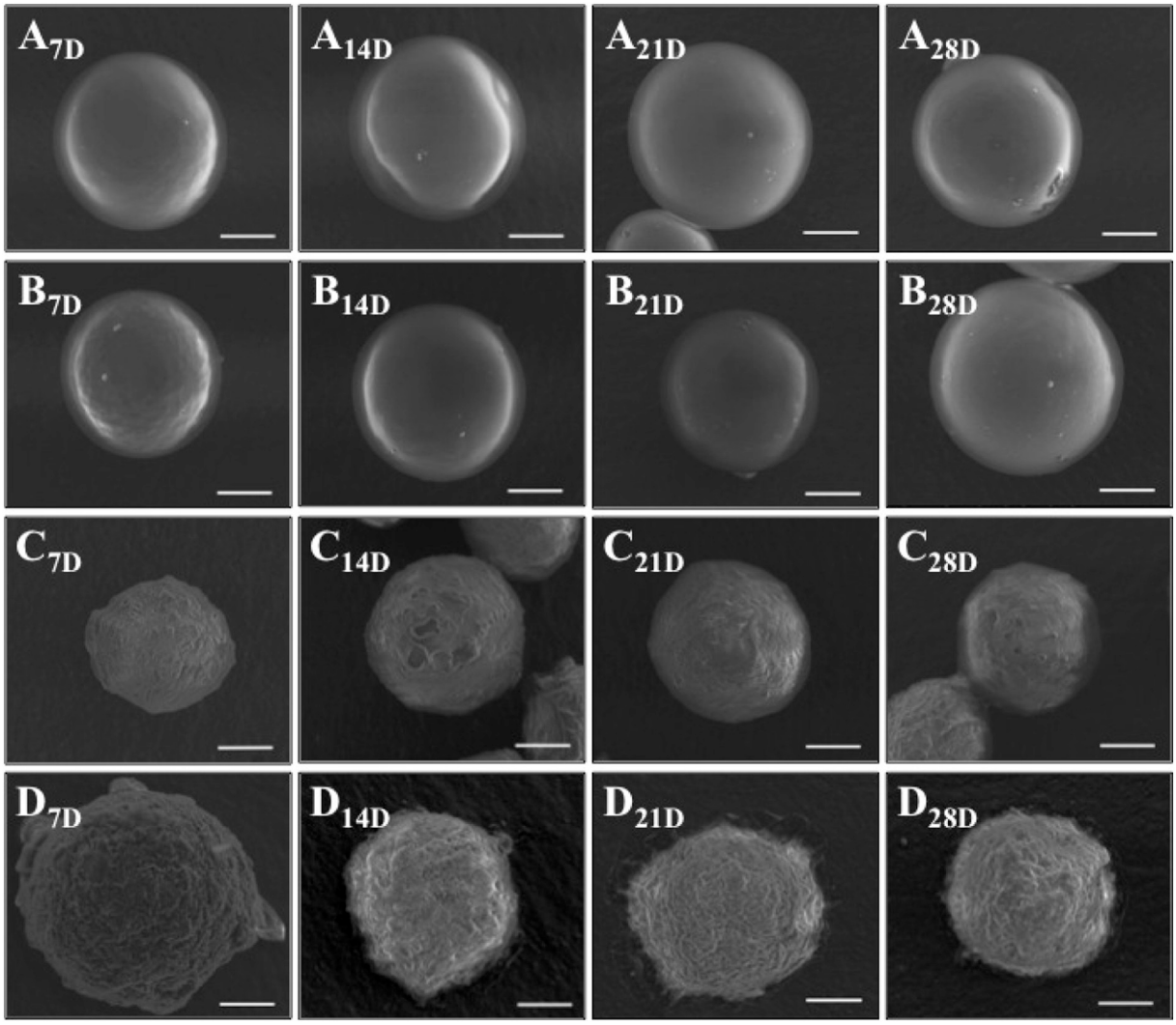

Fig. 6. SEM micrographs of microspheres, after immersion in DMEM-IM at pH = 5 over 28 days. A) RCP; B) RCPfluidMAG-CT; C) $RCPHA_{RT}$; D) RCPFeHA, (Scale bar: 20 μm); (Note: 7D: 7 days; 14D: 14 days; 21D: 21 days; 28D: 28 days).

due to the high microspheres content in the cell culture that negatively affected cell viability. In fact, looking at the absorbance values at day 7, it is clear that they are lower respect to that of 10 μg/mL and 100 μg/mL concentration groups (Fig. 9B).

On the basis of these results, and considering that at day 7 with 100 μg/mL microspheres concentration higher cell viability values without any differences among groups were obtained, this concentration was selected for the further biological investigations.

3.4.2. Cell morphology

Cell morphology was analysed by phalloidin staining and H&E staining. The organization of the cytoskeletal structure of actin filaments is an essential element in maintaining and modulating cellular morphology and cell structural integrity [49]. The morphological analysis made by phalloidin staining showed MC3T3-E1 cells well spread on the well-plate surfaces without any difference among the groups (Fig. 10A). These results were also confirmed by H&E staining by presenting cells well adhered to the surface of the well plate (Fig. 10B). Cells showed their typical polygonal shape and no differences in cell morphology was observed also compared to cells only, proving that the microspheres did not induce any macroscopic negative effect to the cells.

3.4.3. Cell damage evaluation

In order to evaluate the early stage of apoptosis due to the presence of the microspheres in the cell culture, the cellular protein annexin V, commonly used to detect apoptotic cells [50], was investigated at day 1 and after 3 days with an assay that also highlight the presence of necrotic cells. As showed in Fig. 11, RCP, $RCPHA_{RT}$ and RCPFeHA, do not induce cell apoptosis and necrosis. Instead in RCPfluidMAG-CT group few apoptosis and necrosis cells were detected.

A further evaluation was performed to verify if the proposed microspheres could induce the production of reactive oxygen species (ROS), typical index of cell damage [51]. The results indicated that for all the microspheres at both experimental time points, very low level of ROS were produced (Fig. 12), proving that microspheres and the relative ions release do not induce oxidative stress on the cells.

3.4.4. Osteogenic markers evaluation

The effect of 100 μg/mL microspheres on osteogenic related markers induction was evaluated by proteins and mRNA quantification after 7 days of culture. Western blot analysis was performed to evaluate the expression of two osteogenic markers, ALP and osteocalcin, and of the autophagy regulators (LC3B-I and LC3B-II) (Fig. 13). In all the tested microspheres, ALP and osteocalcin were expressed without any significant differences among the groups. A slight increase of LC3B-I and

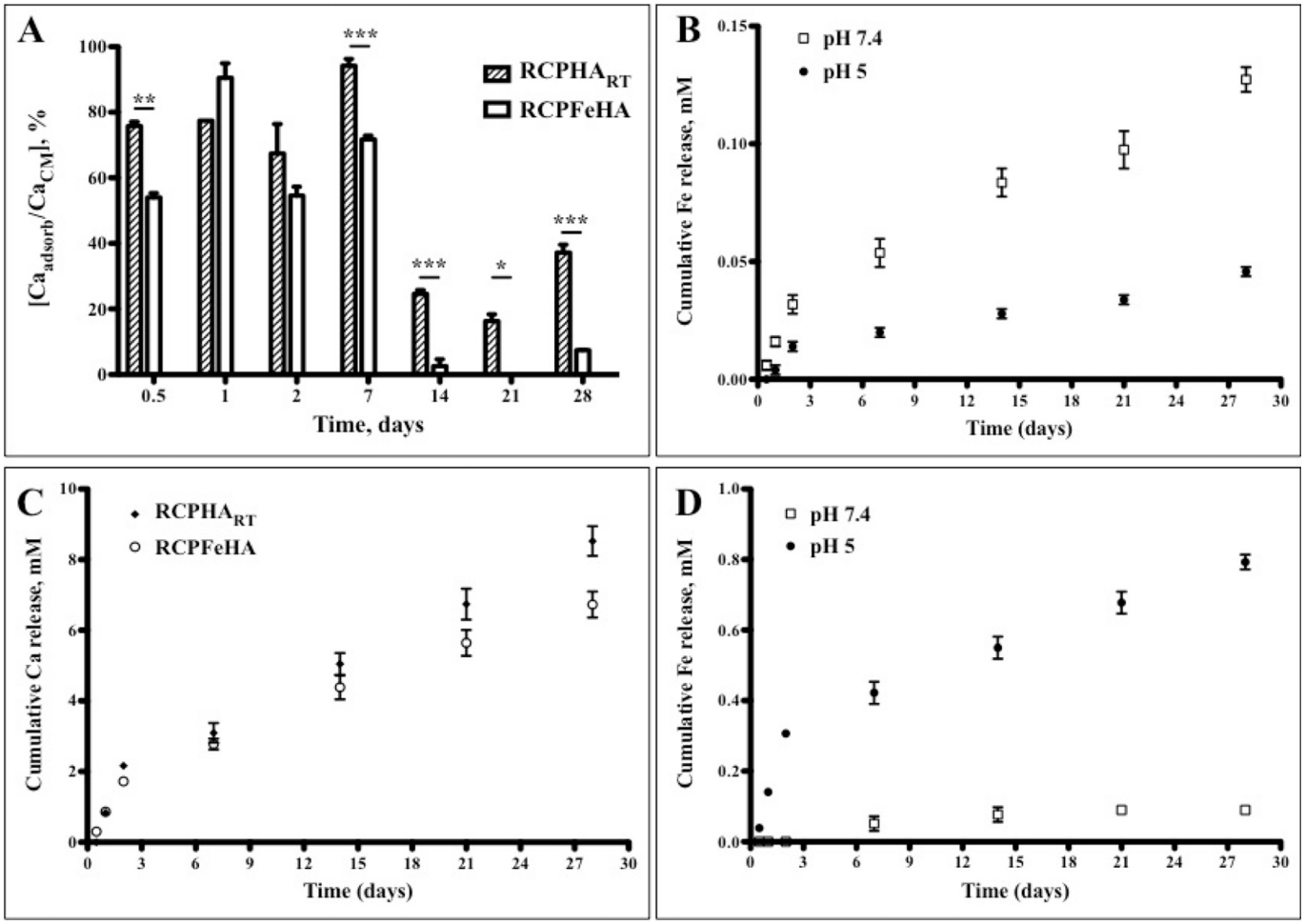

Fig. 7. Adsorption and release of ions from all the tested microspheres. Calcium adsorption (%) by $RCPHA_{RT}$ and RCPFeHA from DMEM at pH 7.4 (A); Cumulative Fe release (mM) from RCPFeHA at pH 7.4 and pH 5 (B); Cumulative Ca release (mM) from $RCPHA_{RT}$ and RCPFeHA at pH 5 (C) and Cumulative Fe release (mM) from RCPfluidMAG-CT (D); ($^{*}p < 0.05$; $^{**}p \leq 0.01$; $^{***}p \leq 0.001$).

LC3B-II, even if without any significant differences, was showed in presence of RCPfluidMAG-CT and RCPFeHA microspheres compared to RCP group.

Moreover, the mRNA level of the osteogenic genes (COL I, SPARC and BGLAP) was evaluate by qPCR (Fig. 14). An overall trend showing an up-regulation of these genes in presence of all hybrid microspheres respect to RCP group was observed. Although, no statistical significant differences were detected among the groups, BGLAP seems to be up-regulated in the entire tested group compared to the RCP, according with protein level results. Instead, RCPFeHA exerted, even weakly, an inductive effect in the expression of COL I and SPARC mRNA level compared to RCPfluidMAG-CT and $RCPHA_{RT}$.

4. Discussion

Biomimetic surface functionalisation of RCPFeHA microspheres opens a new perspective for use as injectable bone fillers with potential ability of drug delivery system with remote magnetic activation.

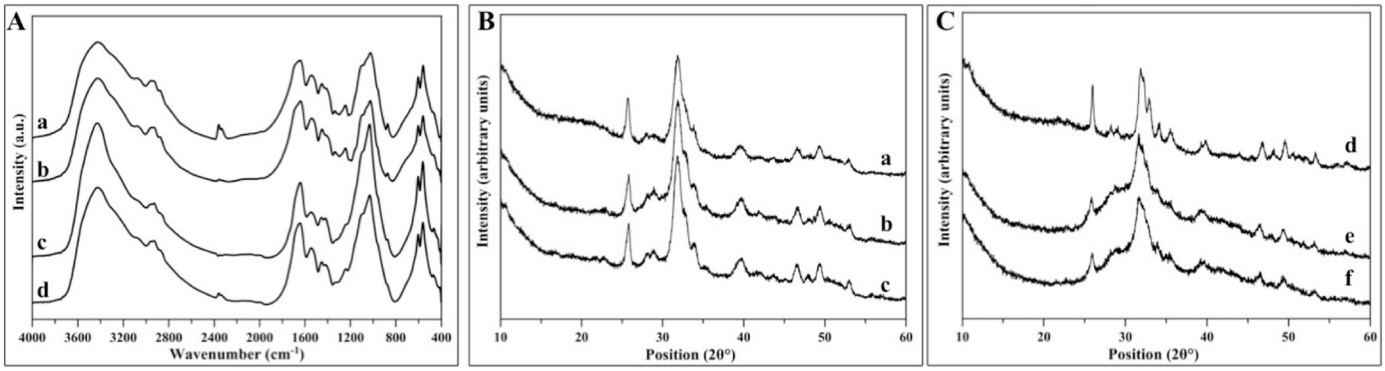

Fig. 8. FTIR spectrum of $RCPHA_{RT}$ after 28 days in pH 7.4 (a) and in pH 5 (b) and RCPFeHA after 28 days at pH 7.4 (c) and at pH 5 (d); (B) XRD pattern of $RCPHA_{RT}$ before (a) and after 28 days at pH 7.4 (b) and pH 5 (c) and of RCPFeHA (C), before (d) and after 28 days at pH 7.4 (e) and pH 5 (f).

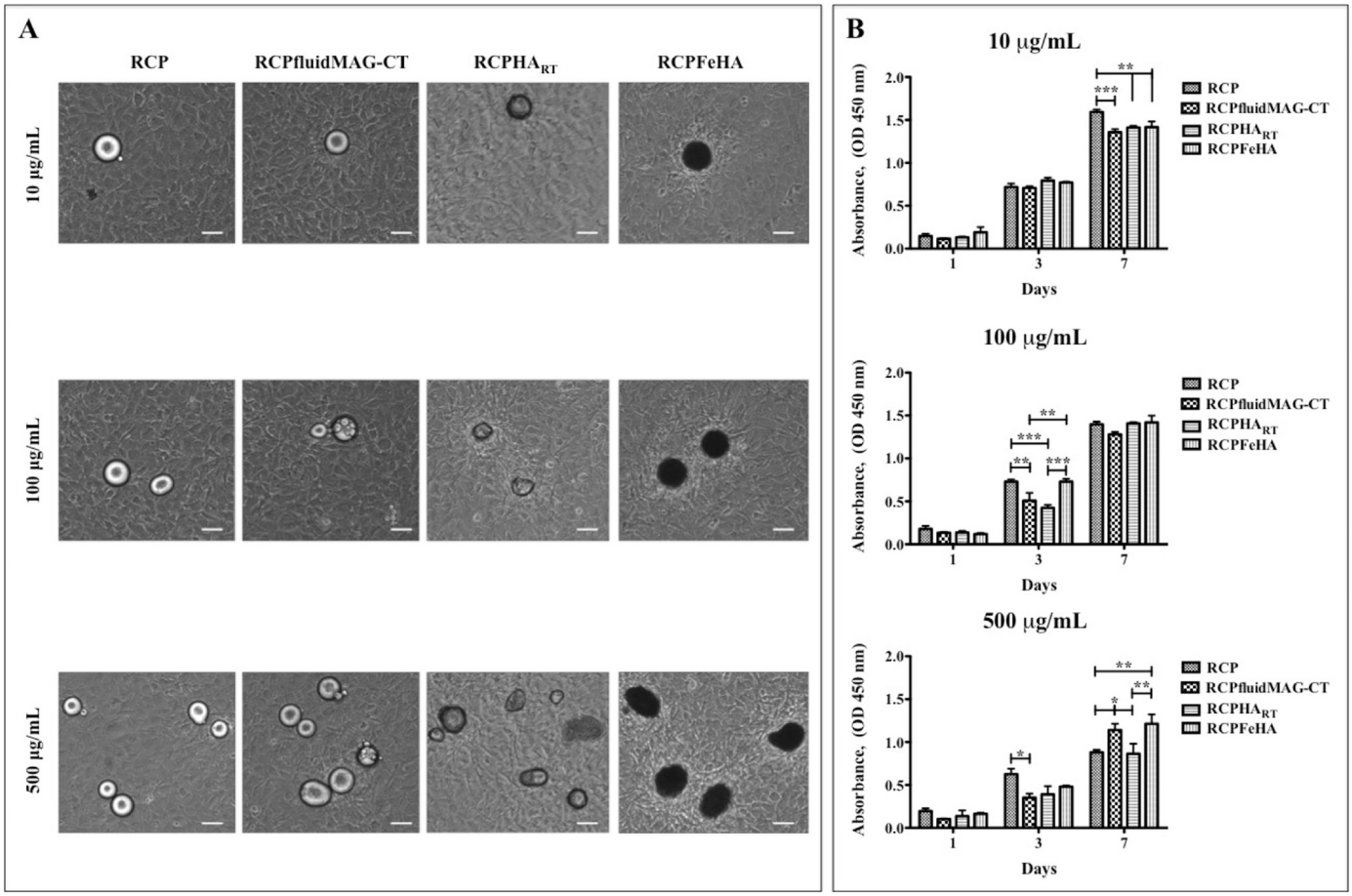

Fig. 9. A) Bright-field images after 7 days of cell culture in presence of all tested microspheres at all tested concentrations (Scale bars: 50 µm). B) Cell viability in presence of all tested microspheres (*$p < 0.05$; **$p < 0.01$; ***$p < 0.001$).

Herein, two types of iron-free mineralised materials were synthesised. In one hand, RCP was mineralised with iron free hydroxyapatite (i.e. RCPHA) at the same conditions of RCPFeHA. Slight differences in crystallinity were ascribed as a factor of influencing rheological behaviour, so that RCPHA was not suitable for microspheres production due to the as-presented low viscosity. As previously discussed [27], iron ions chemically bond the carboxylic groups of RCP polymer, partially replace the calcium ions into apatite lattice and control the crystal

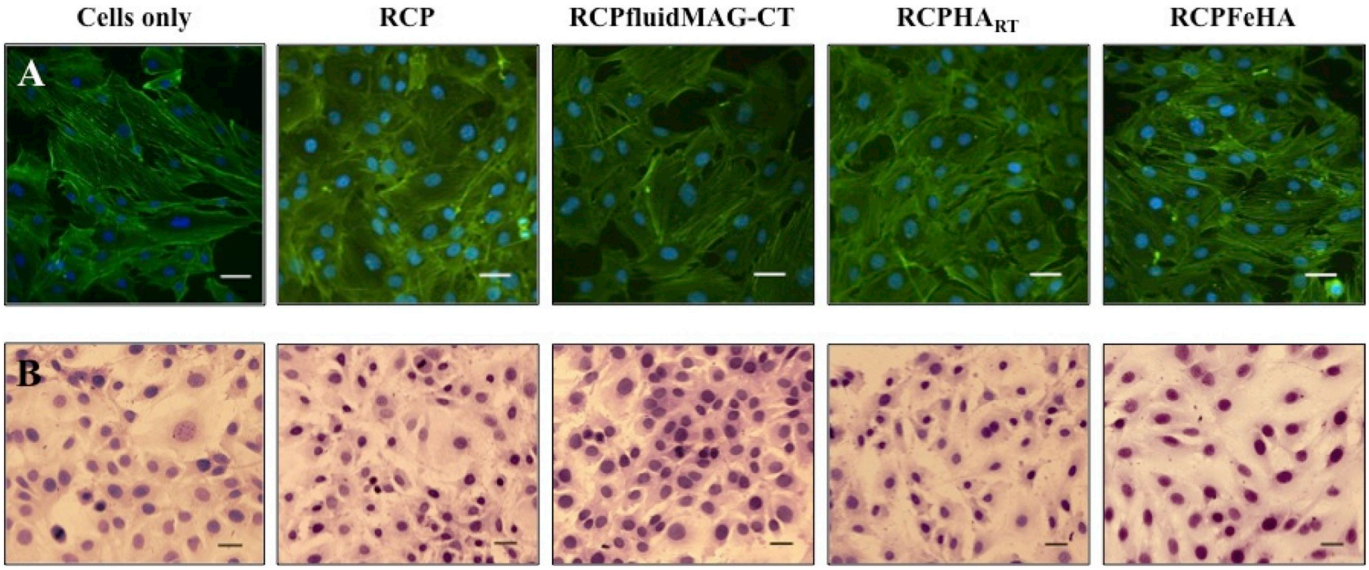

Fig. 10. Morphological analysis of MC3T3-E1 cells cultured at day 3, in presence of 100 µg/mL of microspheres, evaluated by phalloidin staining (green: actin filaments, blue: cell nuclei) (A) and H&E staining (B), (Scale bar: 20 µm). (For interpretation of the references to colour in this figure legend, the reader is referred to the web version of this article.)

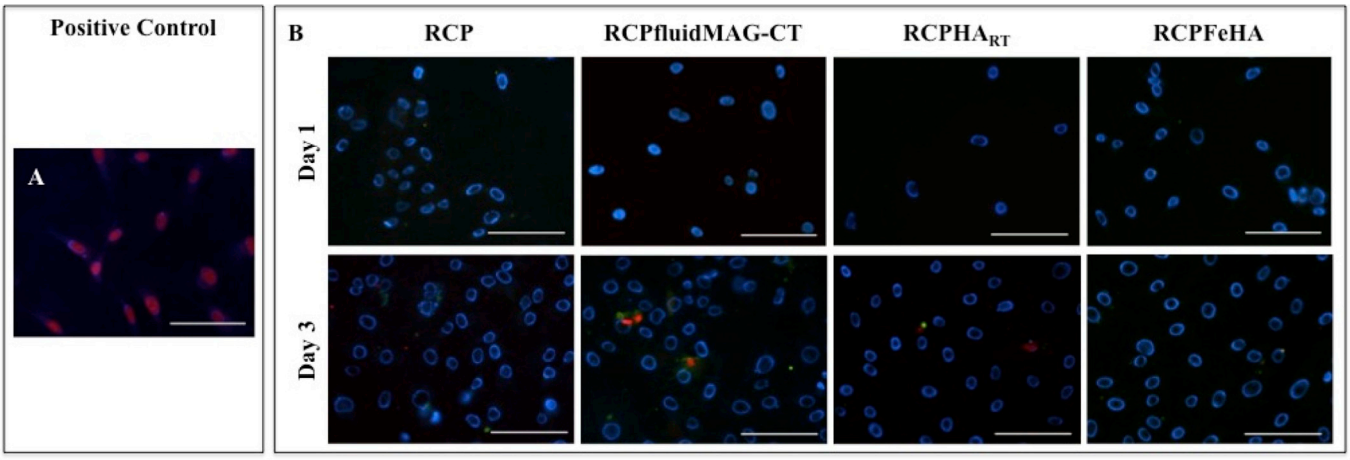

Fig. 11. A) Positive control; B) Effect of microspheres on cells apoptosis/necrosis, at concentration of 100 μg/mL and at two experimental time points (Day 1 and Day 3). Apoptotic cells in green, necrotic cells in red, cell nuclei in blue, (Scale bar: 50 μm). (For interpretation of the references to colour in this figure legend, the reader is referred to the web version of this article.)

growth. Those phenomena improve the viscosity of iron doped mineralised slurries, thus microspheres with well-defined shape and size can be obtained. In the case of iron-free microspheres, to obtain viscosity suitable for the emulsification of the slurries into carriers suitable for biomedical applications, the synthesis temperature has to be lowered to obtain mineral phase with lower crystallinity, such as RCPHA$_{RT}$.

Citrate was used to functionalise RCPHA$_{RT}$ and RCPFeHA microspheres. Citrate is present in bone tissue and plays an active role to complex calcium ions, and to control the crystal growth of the mineral bone. Moreover, it controls the agglomeration phenomena thanks to the high affinity of citrate ions with positively charged calcium and iron ions exposed on the apatite surface, thus representing an interesting candidate as bioactive functionalising agent for CaP-based hybrid magnetic microspheres.

All the tested microspheres were stable at both physiological and inflammatory-mimicking conditions, up to 28 days of investigation. The use of a recombinant biopolymer enriched of RGD motifs, able to induce bio-inspired mineralisation with bioactive mineral phase, can result into enhanced chemical and biological cues for cells, fuelling new bone formation and tissue regeneration. In this respect, magnetic RCPFeHA is of particular interest, due to the release of both calcium and iron ions that further can support bone homeostasis and regeneration, also in the case of degenerative diseases such as osteoporosis [3,4,52,53]. In physiological mimicking conditions, the low crystallinity of RCPFeHA microspheres allowed the adsorption of calcium ions from the DMEM and establishes an ion exchange process yielding the release of iron ions to the cells. On the other hand, the dissolution of RCPFeHA microspheres in inflammatory-mimicking conditions can make available both Ca and Fe ions. Therefore, RCPFeHA microspheres can be considered as stimuli-responsive devices delivering cell-instructing cues useful for bone repair, particularly when pathological conditions related to tumour, bone damage or fractures elicit the activation of pro-inflammatory states [54,55].

The effect of non-mineralised and mineralised microspheres on cell viability, cell morphology and their ability on promoting osteogenic differentiation of MC3T3-E1 cells were evaluated. All the tested microspheres were cytocompatible, without apoptotic activation or reactive oxygen species production in exception of RCPfluidMAG-CT, which however was not obtained by bio-inspired mineralisation, but by simple mixing with an iron oxide phase. This confirms that the constraints exerted on the mineral phase during heterogeneous nucleation guided by a natural biopolymer, typical of bio-inspired mineralisation process, drive the formation of hybrid nanomaterials with bio-mimicking physico-chemical and ultrastructural features more suitable for cells, thus improving tissue healing. This assumption is further supported by the morphology of seeded cells, well considered as an index

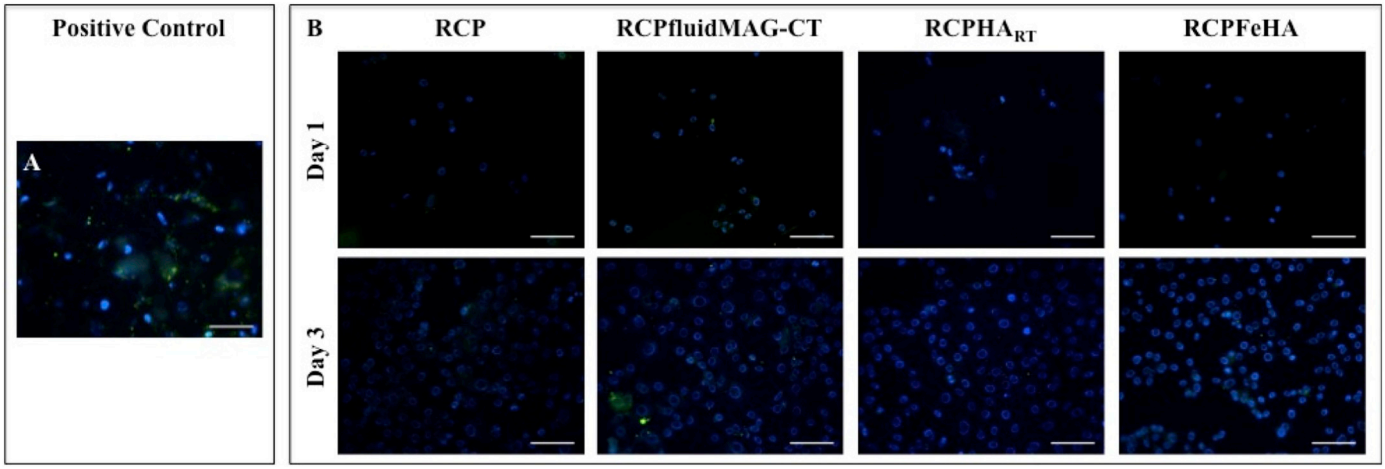

Fig. 12. A) Positive control; C) Effect of microspheres on ROS production, at concentration of 100 μg/mL and at two experimental time points (Day 1 and Day 3), (Scale bar: 50 μm).

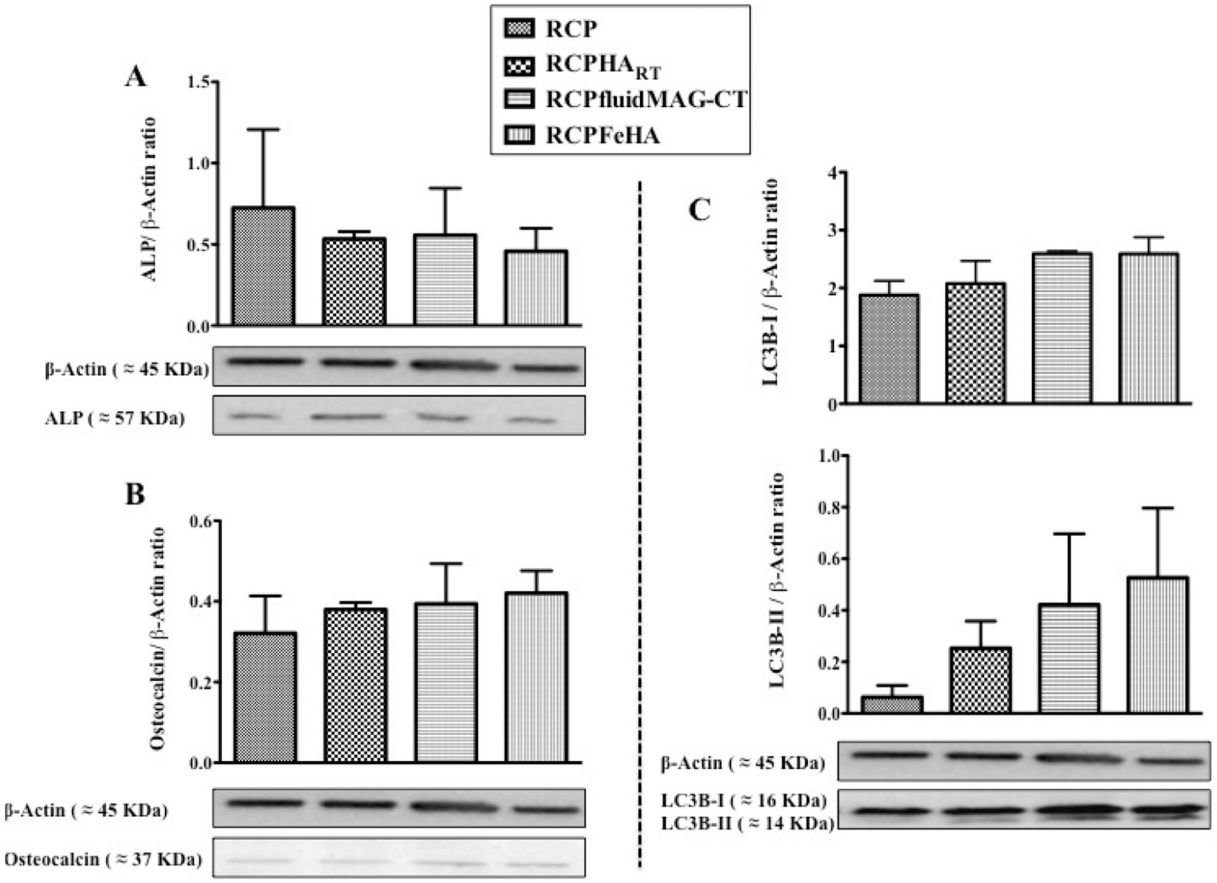

Fig. 13. Western blot analysis at day 7 for ALP (A), osteocalcin (B) and autophagy marker (C) LC3B-I (graph above) and LC3B-II (graph below). β-Actin was used as an internal control.

of cell activity [56], showing very good adhesion and spreading, thus confirming the absence of any cytotoxic effects from all the tested microspheres.

The ability of microspheres compositions to stimulate the expression of osteogenic markers from MC3T3-E1 was also evaluated in this study. Although weakly, a trend of induction exerted by RCPFeHA microspheres in all the tested markers was observed, which can be correlated with the presence of iron ions in the cell culture medium, as a result of ion exchange and microspheres dissolution. Hence, we can hypothesize that the features of hybrid microspheres, particularly RCPFeHA, induce sustained expression of osteogenic markers also in the long term, particularly related to the continuous release of iron ions in the cell culture medium. In this respect, the high proliferative activity detected after 7 days of culture as induced by all the microspheres can justify the absence of strong osteogenic differentiation stimulus in the first week of culture, as reported in [57].

5. Conclusions

The versatility of bio-inspired mineralisation process used to generate hybrid microspheres with bioactive composition and adequate dispersion ability in physiological media, allowed to achieve promising hybrid materials as microcarriers with stimuli-responsive ability. The use of bioactive citrate ions was showed to improve microspheres production and in delivering cell-instructing signals by different release mechanisms, acting in physiological and inflammatory pH-mimicking

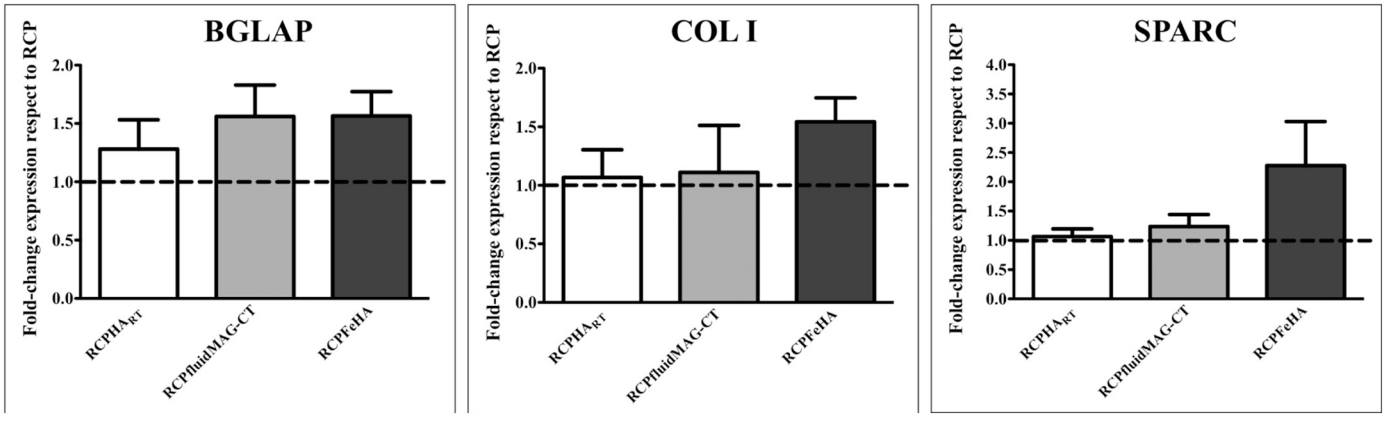

Fig. 14. Relative quantification ($2^{-\Delta\Delta Ct}$) of osteogenic related genes expression after 7 days of MC3T3-E1 culture with all the tested microspheres.

conditions, thus positively influencing the expression of osteogenic markers. Furthermore, superparamagnetic properties shown by hybrid microspheres such as RCPFeHA can enable further control of the bioactivity and functionality. Hybrid magnetic biomaterials are increasingly considered as new generation of bio-devices associating biomimicry and ability of remote activation and release of bioactive molecules along defined spatial-temporal profiles, thus responding to the ever-increasing need of personalized, more targeted and effective therapies in regenerative medicine.

Acknowledgments

The authors acknowledge Dr. Samuele Dozio for helping in biological tests and to Fujifilm Manufacturing Europe B.V. (The Netherlands) for providing the Cellnest™.

Funding

The research leading to these results has received funding from the European Union Seventh Framework Programme FP7-PEOPLE-2013-ITN under grant agreement no. 607051.

Appendix A. Supplementary data

Supplementary data to this article can be found online at https://doi.org/10.1016/j.msec.2018.11.014.

References

[1] M.T. Lopez-Lopez, et al., Generation and characterization of novel magnetic field-responsive biomaterials, PLoS One 10 (2015) 1–17.
[2] R.K. Singh, et al., Potential of magnetic nanofiber scaffolds with mechanical and biological properties applicable for bone regeneration, PLoS One 9 (2014).
[3] R.A. Perez, et al., Therapeutically relevant aspects in bone repair and regeneration, Mater. Today 18 (2015) 573–589.
[4] Q. Wang, J. Yan, J. Yang, B. Li, Nanomaterials promise better bone repair, Mater. Today 19 (2016) 451–463.
[5] A.R. Amini, C.T. Laurencin, S.P. Nukavarapu, Bone tissue engineering: recent advances and challenges, Crit. Rev. Biomed. Eng. 40 (2012) 363–408.
[6] S. Panseri, et al., Magnetic labelling of mesenchymal stem cells with iron-doped hydroxyapatite nanoparticles as tool for cell therapy, J. Biomed. Nanotechnol. 12 (2016) 909–921.
[7] G.S. Krishnakumar, et al., Ribose mediated crosslinking of collagen-hydroxyapatite hybrid scaffolds for bone tissue regeneration using biomimetic strategies, Mater. Sci. Eng. C 77 (2017) 594–605.
[8] M. Montesi, S. Panseri, M. Iafisco, A. Adamiano, A. Tampieri, Coupling hydroxyapatite nanocrystals with lactoferrin as a promising strategy to fine regulate bone homeostasis, PLoS One 10 (2015) e0132633.
[9] G.B. Ramírez-Rodríguez, et al., Biomineralized recombinant collagen-based scaffold mimicking native bone enhances mesenchymal stem cell interaction and differentiation, Tissue Eng. Part A 23 (2017) 1423–1435.
[10] G. Calabrese, et al., Collagen-hydroxyapatite scaffolds induce human adipose derived stem cells osteogenic differentiation in vitro, PLoS One 11 (2016) 1–17.
[11] B. Grigolo, et al., Novel nano-composite biomimetic biomaterial allows chondrogenic and osteogenic differentiation of bone marrow concentrate derived cells, J. Mater. Sci. Mater. Med. 26 (173) (2015).
[12] J. Gustavsson, M.P. Ginebra, E. Engel, J. Planell, Ion reactivity of calcium-deficient hydroxyapatite in standard cell culture media, Acta Biomater. 7 (2011) 4242–4252.
[13] A. Tampieri, et al., A conceptually new type of bio-hybrid scaffold for bone regeneration, Nanotechnology 22 (2011) 15104.
[14] S. Bose, S. Tarafder, Calcium phosphate ceramic systems in growth factor and drug delivery for bone tissue engineering: a review, Acta Biomater. 8 (2012) 1401–1421.
[15] M. Montesi, S. Panseri, M. Dapporto, A. Tampieri, S. Sprio, Sr-substituted bone cements direct mesenchymal stem cells, osteoblasts and osteoclasts fate, PLoS One 12 (2017) e0172100.
[16] (B) S. Sprio et al. Bio-inspired assembling/mineralization process as a flexible approach to develop new smart scaffolds for the regeneration of complex anatomical regions. J. Eur. Ceram. Soc. 36, 2857–2867.
[17] A. Tampieri, S. Sprio, M. Sandri, F. Valentini, Mimicking natural bio-mineralization processes: a new tool for osteochondral scaffold development, Trends Biotechnol. 29 (2011) 526–535.
[18] A. Tampieri, et al., Intrinsic magnetism and hyperthermia in bioactive Fe-doped hydroxyapatite, Acta Biomater. 8 (2012) 843–851.
[19] V. Iannotti, et al., Fe-doping-induced magnetism in nano-hydroxyapatites, Inorg. Chem. 56 (2017) 4446–4458.
[20] S. Panseri, et al., Intrinsically superparamagnetic Fe-hydroxyapatite nanoparticles positively influence osteoblast-like cell behaviour, J. Nanobiotechnol. 10 (2012) 32.
[21] S. Gil, J.F. Mano, Magnetic composite biomaterials for tissue engineering, Biomater. Sci. 2 (2014) 812–818.
[22] L.J. Santos, R.L. Reis, M.E. Gomes, Harnessing magnetic-mechano actuation in regenerative medicine and tissue engineering, Trends Biotechnol. 33 (2015) 471–479.
[23] B. Sarker, et al., Evaluation of fibroblasts adhesion and proliferation on alginate-gelatin crosslinked hydrogel, PLoS One 9 (2014) 1–12.
[24] H.-M. Yun, et al., Magnetic nanocomposite scaffolds combined with static magnetic field in the stimulation of osteoblastic differentiation and bone formation, Biomaterials 85 (2016) 88–98.
[25] J. Meng, et al., Super-paramagnetic responsive nanofibrous scaffolds under static magnetic field enhance osteogenesis for bone repair in vivo, Sci. Rep. 3 (2655) (2013).
[26] A. Tampieri, et al., Magnetic Bioinspired Hybrid Nanostructured Collagen − Hydroxyapatite Scaffolds Supporting Cell Proliferation and Tuning Regenerative Process, (2014).
[27] T. Patrício, S. Panseri, M. Sandri, A. Tampieri, S. Sprio, New bioactive bone-like microspheres with intrinsic magnetic properties obtained by bio-inspired mineralisation process, Mater. Sci. Eng. C 77 (2017) 613–623.
[28] R. Pareta, E. Taylor, T. Webster, Increased osteoblast density in the presence of novel calcium phosphate coated magnetic nanoparticles, Nanotechnology 19 (2008) 265101.
[29] C. Marques, et al., Multifunctional materials for bone cancer treatment, Int. J. Nanomedicine 9 (2014) 2713–2725.
[30] M.P. Ginebra, C. Canal, M. Espanol, D. Pastorino, E.B. Montufar, Calcium phosphate cements as drug delivery materials, Adv. Drug Deliv. Rev. 64 (2012) 1090–1110.
[31] H.J. Lee, H.W. Choi, K.J. Kim, S.C. Lee, Modification of hydroxyapatite nanosurfaces for enhanced colloidal stability and improved interfacial adhesion in nanocomposites, Chem. Mater. (2006), https://doi.org/10.1021/cm061139x.
[32] A. Ashokan, D. Menon, S. Nair, M. Koyakutty, A molecular receptor targeted, hydroxyapatite nanocrystal based multi-modal contrast agent, Biomaterials (2010), https://doi.org/10.1016/j.biomaterials.2009.11.113.
[33] Y. Han, X. Wang, S. Li, A simple route to prepare stable hydroxyapatite nanoparticles suspension, J. Nanopart. Res. (2009), https://doi.org/10.1007/s11051-008-9507-8.
[34] S.C. Liou, S.Y. Chen, D.M. Liu, Manipulation of nanoneedle and nanosphere apatite/poly (acrylic acid) nanocomposites, J Biomed Mater Res B Appl Biomater (2005), https://doi.org/10.1002/jbm.b.30193.
[35] H. Liu, E.B. Slamovich, T.J. Webster, Less harmful acidic degradation of poly(lactic-co-glycolic acid) bone tissue engineering scaffolds through titania nanoparticle addition, Int. J. Nanomedicine 1 (2006) 541–545.
[36] J.M. Delgado-López, et al., Crystallization of bioinspired citrate-functionalized nanoapatite with tailored carbonate content, Acta Biomater. 8 (2012) 3491–3499.
[37] M. Iafisco, et al., The growth mechanism of apatite nanocrystals assisted by citrate: relevance to bone biomineralization, CrystEngComm 17 (2015) 507–511.
[38] L.C. Costello, M. Chellaiah, J. Zou, R.B. Franklin, M.A. Reynolds, HHS public access, J. Regen Med. Tissue Eng. 3 (2014).
[39] B. Sandhöfer, et al., Synthesis and preliminary in vivo evaluation of well-dispersed biomimetic nanocrystalline apatites labeled with positron emission tomographic imaging agents, ACS Appl. Mater. Interfaces 7 (2015) 10623–10633.
[40] V. Di Mauro, et al., Bioinspired negatively charged calcium phosphate nanocarriers for cardiac delivery of MicroRNAs, Nanomedicine 11 (2016) 891–906.
[41] K.J. Livak, T.D. Schmittgen, Analysis of relative gene expression data using real-time quantitative PCR and the $2^{-\Delta\Delta CT}$ method, Methods 25 (2001) 402–408.
[42] Y. Liu, J. Lim, S.H. Teoh, Review: development of clinically relevant scaffolds for vascularised bone tissue engineering, Biotechnol. Adv. 31 (2013) 688–705.
[43] K.N. Ivey, et al., MicroRNA regulation of cell lineages in mouse and human embryonic stem cells, Cell Stem Cell 2 (2008) 219–229.
[44] A.I. Mitsionis, T.C. Vaimakis, C.C. Trapalis, The effect of citric acid on the sintering of calcium phosphate bioceramics, Ceram. Int. 36 (2010) 623–634.
[45] E. Cheraghipour, S. Javadpour, A.R. Mehdizadeh, Citrate capped superparamagnetic iron oxide nanoparticles used for hyperthermia therapy, J. Biomed. Sci. Eng. 5 (2012) 715–719.
[46] S. Weiner, O. Bar-Yosef, States of preservation of bones from prehistoric sites in the near east: a survey, J. Archaeol. Sci. 17 (1990) 187–196.
[47] T. Surovell, M. Stiner, Standardizing infra-red measures of bone mineral crystallinity: an experimental approach, J. Archaeol. Sci. 28 (2001) 633–642.
[48] S. Guicciardi, et al., Rheological characteristics of slurry controlling the microstructure and the compressive strength behavior of biomimetic hydroxyapatite, J. Mater. Res. 16 (2001) 163–170.
[49] M. Radulovic, J. Godovac-Zimmermann, Proteomic approaches to understanding the role of the cytoskeleton in host-defense mechanisms, Expert Rev. Proteomics 8 (2011) 117–126.
[50] G. Koopman, et al., Annexin V for flow cytometric detection of phosphatidylserine expression on B cells undergoing apoptosis, Blood 84 (1994) 1415–1420.
[51] G. Stark, Functional consequences of oxidative membrane damage, J. Membr. Biol. 205 (2005) 1–16.
[52] S.K. Boda, G. Thrivikraman, B. Panigrahy, D.D. Sarma, B. Basu, Competing Roles of Substrate Composition, Microstructure, and Sustained Strontium Release in Directing Osteogenic Differentiation of hMSCs, ACS Appl. Mater. Interfaces (2016), https://doi.org/10.1021/acsami.6b08694 (acsami.6b08694).
[53] L. Toxqui, M.P. Vaquero, Chronic iron deficiency as an emerging risk factor for osteoporosis: a hypothesis, Nutrients 7 (2015) 2324–2344.
[54] M. Nakamura, R. Hiratai, T. Hentunen, J. Salonen, K. Yamashita, Hydroxyapatite with high carbonate substitutions promotes osteoclast resorption through osteocyte-like cells, ACS Biomater. Sci. Eng. 2 (2016) 259–267.
[55] T.R. Arnett, Acidosis, hypoxia and bone, Arch. Biochem. Biophys. 503 (2010) 103–109.
[56] K. Lin, et al., Tailoring the nanostructured surfaces of hydroxyapatite bioceramics to promote protein adsorption, osteoblast growth, and osteogenic differentiation, ACS Appl. Mater. Interfaces 5 (2013) 8008–8017.
[57] S. Ruijtenberg, S. van den Heuvel, Coordinating cell proliferation and differentiation: antagonism between cell cycle regulators and cell type-specific gene expression, Cell Cycle (2016), https://doi.org/10.1080/15384101.2015.1120925.